Title: Transcriptional competition shapes proteotoxic ER stress resolution

Authors: Dae Kwan Ko[1,3], Federica Brandizzi[1,2,3*]

Affiliations:

[1]MSU-DOE Plant Research Lab, Michigan State University, East Lansing, Michigan, 48824

[2]Department of Plant Biology, Michigan State University, East Lansing, Michigan, 48824

[3]Great Lakes Bioenergy Research Center, Michigan State University, East Lansing, Michigan, 48824

*Corresponding author. Email: fb@msu.edu

Through dynamic activities of conserved master transcription factors (mTFs), the unfolded protein response (UPR) relieves proteostasis imbalance of the endoplasmic reticulum (ER), a condition known as ER stress[1,2]. Because dysregulated UPR is lethal, the competence for fate changes of the UPR mTFs must be tightly controlled[3,4]. However, the molecular mechanisms underlying regulatory dynamics of mTFs remain largely elusive. Here, we identified the abscisic acid (ABA)-related regulator G-class bZIP TF2 (GBF2) and the *cis*-regulatory element G-box as regulatory components of the plant UPR led by the mTFs, bZIP28 and bZIP60. We demonstrate that, by competing with the mTFs at G-box, GBF2 represses UPR gene expression. Conversely, a *gbf2* null mutation enhances UPR gene expression and suppresses the lethality of a *bzip28 bzip60* mutant in unresolved ER stress. By demonstrating that GBF2 functions as a transcriptional repressor of the UPR, we address the long-standing challenge of identifying shared signaling components for a better

understanding of the dynamic nature and complexity of stress biology. Furthermore, our results identify a new layer of UPR gene regulation hinged upon an antagonistic mTFs-GFB2 competition for proteostasis and cell fate determination.

Dynamic reprogramming of gene expression is universally important for stress responses[5] and is orchestrated primarily by TFs that regulate target genes by binding short DNA sequences on the genome, known as *cis*-regulatory elements (CREs)[6]. The gene regulatory activity of a TF is often controlled by an interplay with one or multiple regulators, such as other TFs[7], which also regulate other target genes in concert with other regulators, generating a complex biological network web known as gene regulatory network (GRN)[8]. Timely managed gene expression changes in response to environmental stress are possible through GRNs[9]. One of the well-known phenomena governed by GRN is the UPR[3,4], a protein quality control signaling network designed to protect organisms from endogenous and induced stress that alters ER proteostasis[1,2]. The UPR senses increases in the accumulation of unfolded or misfolded proteins in the ER and reprograms gene expression associated with protein folding and diverse biological processes, including cell fate determination[4,10]. In *Arabidopsis thaliana* (hereafter Arabidopsis), UPR gene regulation is tightly controlled by bZIP28 and bZIP60, two functionally conserved mTFs that bind UPR gene promoters specifically via CREs, including the highly conserved ER stress-responsive element I (ERSE-I)[4,11]. Understanding the regulatory mechanisms for the coordination of dynamic gene expression by bZIP28 and bZIP60 is a central challenge due to their partial functional redundancy[1,2,4,12] and the multi-functionality of TFs in general[6,13,14].

TFs are generally associated with multiple pathways in growth and stress responses[13,14]. Similarly, UPR regulators function in diverse pathways, as demonstrated earlier[3,15-17]. Identification of signaling factors shared across pathways is one of the main challenges in

45 understanding the dynamic complexity of growth and stress management. To identify regulators
46 shared with the UPR, we adopted transcriptome profiles at 0 h, 12 h and 24 h following removal
47 of tunicamycin (Tm), an ER stress inducer, which was administered to seedlings for 6 h[4].
48 Therefore, 0 h corresponds to a peak in adaptive UPR during which ER chaperone genes are
49 upregulated[4,12]. Notably, upon Tm wash-out at 0 h, through processes collectively coined ER stress
50 recovery (ERR), ER stress and adaptive UPR are progressively mitigated, and growth is
51 resumed[4,12]. We compared these transcriptomes to those of seedlings treated with the
52 phytohormone abscisic acid (ABA)[13], which we selected because it is involved in a variety of
53 processes, including stress responses, development and metabolism[13]. We found that 22%
54 (928/4213) of differentially expressed genes (DEGs) in ERR were also differentially expressed in
55 ABA treatment with a significant overlap ($P = 5.18 \times 10^{-172}$) (Fig. 1a, Extended Data Fig. 1a and
56 Supplementary Data 1), hereafter ERR-ABA DEGs, and were associated with significant
57 biological pathways, including stress responses, growth and metabolism (Extended Data Fig. 1b
58 and Supplementary Data 2). Moreover, the relative gene expression changes were temporally and
59 dynamically correlated between ABA and ERR when DEGs were compared between each time
60 point of ABA and ERR treatment (significant positive correlation at 0 h of ER stress recovery with
61 4 h, 8 h, 12 h, 24 h and 36 h of ABA) (Fig. 1b and Extended Data Fig. 2). These results support
62 the existence of a temporal regulatory link between at least two stress-induced gene
63 reprogramming pathways, which are potentially regulated by common regulatory factors, such as
64 TFs. The presence of specific CREs on the gene promoters often determines their activity (e.g., by
65 generating interactions among TFs) and may lead to stress-responsive gene expression[13,18]. To
66 identify potential CREs enriched in the promoters of ERR-ABA DEGs, we performed *de novo*
67 motif analyses of 10 individual overlapping promoters (~100-bp long) spanning 1-kb promoters

(named as Fragment 1 to 10) of ERR-ABA DEGs (Extended Data Fig. 3). We identified six significantly enriched potential CREs exclusively on either Fragment 3, 4, 5, 8, 9 or 10 (Fig. 1c). These CREs significantly match with binding motifs of distinct TF families: CXC-hinge-CXC, C2C2 DOF, bZIP, WRKY, MYB and C2C2 DOF on Fragment 3, 4, 5, 8, 9 or 10, respectively (Supplementary Data 3). These results suggest that multiple CREs present on specific locations in the gene promoters may regulate gene expression in response to both ABA and ER stress treatments. Among the potential CREs, G-box (CACGT) significantly enriched on the Fragment 9 (-200-bp to -90-bp) attracted our attention because it is known as bZIP TF binding site[19] and its core sequence (CACG; known as ABSCISIC ACID RESPONSIVE ELEMENT [ABRE]) is contained in the second subunit (underlined) of ERSE-I (CCAAT-N_{10}-<u>CACG</u>). Surprisingly, all core UPR genes contain multiple copies of G-box/ABRE on either the 1-kb promoters or 5'UTR sequences (Extended Data Fig. 4), collectively supporting that G-box is likely a new CRE that modulates gene expression in the UPR.

Next, to identify the corresponding *trans*-acting elements (i.e., TFs) of the G-box, we performed a large-scale enhanced yeast one-hybrid (eY1H) screen[20,21] with two ~550-bp-long partially overlapping fragments (Fa, fragment a [away from transcription start site]; Fb, fragment b [containing the transcription start site]) spanning the 1-kb promoters of *bZIP28*, *bZIP60* and *BiP3* (Fig. 1d and Supplementary Table 1). *BiP3* is a transcriptional target of bZIP28 and bZIP60[4,11,12,22,23] and, due to its robust transcriptional response to ER stress, is the most representative UPR marker gene encoding a highly conserved ER chaperone[1,24]. We reasoned that these UPR genes would be dynamically regulated under ER stress and other stress[2], and likely targeted by multi-functional TFs in specific gene regulatory modules linking the UPR to other biological pathways for ER homeostasis, as shown for the maize UPR[3]. Therefore, we screened

the six promoter fragments from the three UPR genes against a collection of ~2,000 Arabidopsis TFs. We identified a total of 603 protein-DNA interactions (PDIs) and nonredundant 285 binding TFs (141, *BiP3*; 200, *bZIP28*; 121, *bZIP60*) (Fig. 1e and Supplementary Data 4). The PDIs were likely DNA sequence-specific as supported by binding enrichments of specific TF families on either promoter fragment (Fa or Fb) with an exclusive presence of the corresponding binding sites (Extended Data Fig. 5). A TF network map based on 471 PDIs (gene-TF) coupled with the temporal expression of each TF in ERR[4] revealed a high level of regulatory redundancy of these UPR genes and regulatory modules in which TFs co-bound either single or multiple UPR genes (Fig. 1f). We found that TF genes in each regulatory cluster (i.e., TFs binding exclusively to a single gene or multiple genes) were enriched with diverse biological pathways, including responses to hormones-related pathways (Extended Data Fig. 6 and Supplementary Data 5), supporting our rationale that UPR regulators could be involved also in other stress responses. We next aimed to validate these PDIs and investigate gene involvement in cell fate under ER stress. We selected 12 TFs based on their association with abiotic stress or hormone response and membership to the regulatory clusters (Fig. 1f and Extended Data Fig. 7), and we scored the relative root length elongation of transcriptional knock-out mutants (KOs), as a hallmark of ERR after Tm wash-out[12]. Single and double KOs of *bZIP28* and *bZIP60* (*bzip28-2, bzip60-2* and *bzip28-2 bzip60-1*) showed significantly reduced relative growth of primary root in ERR compared to Col-0, consistent with previous studies[4,12]. The selected TF KOs showed no significant differences in primary root growth relative to Col-0, presumably due to functional redundancy[13], with the exception of a *GBF2* KO, which displayed a significant hyposensitivity to ER stress, as verified for three independent KO alleles (*gbf2-1*, *gbf2-2* and *gbf2-3*) (Fig. 2a,b and Extended Data Fig. 7). Interestingly, a KO of *GBF3*, a bZIP TF gene partially redundant with *GBF2* in vascular

development[25], showed no difference in the root growth, suggesting functional diversification among the GBF TF family. Consistent with this hypothesis, a double *GBF1*, *GBF3* KO [*gbf1* (-/-) *gbf2-2* (-/+) *gbf3* (-/-)[25] (a triple mutant could not be recovered in this study)] also showed no difference in the root growth relative to Col-0 (Extended Data Fig. 7).

GBF2 is an ABA-responsive TF that binds hundreds of genes via G-box[13,26], which temporally regulates gene expression in response to ABA (Extended Data Fig. 8) and physically interacts with the bZIP TF HY5[27], a negative regulator of the UPR[16]. To profile genome-wide *in vivo* DNA-binding activities of GBF2 in the UPR, we performed chromatin immunoprecipitation sequencing (ChIP-seq) analyses of GBF2 at 0 h of ERR (i.e., 6 h of Tm treatment or DMSO) using a *GBF2* native promoter-driven yellow fluorescent protein for energy transfer (Ypet)-tagged *GBF2* line (*pGBF2*:*GBF2-Ypet*)[13]. Our analysis pipeline generated 523 Tm sample-specific binding peaks of GBF2 (i.e., not overlapped with peaks found in the corresponding DMSO-treated samples; see Methods) (Fig. 2c and Supplementary Data 6). Hereafter we refer to these peaks as UPR-specific binding peaks. We found that the majority of UPR-specific binding peaks (77.25%) were located in the proximal gene promoters (i.e., within 1-kb of the transcription start site) (Fig. 2c), consistent with typical activities of other Arabidopsis TFs[28]. *De novo* motif analysis revealed G-box as the top-scoring motif (E-value = 4.5×10^{-79}) in UPR-specific binding peaks (Fig. 2d), validating the high quality of our data. We next mapped GBF2 UPR-specific binding peaks to the gene targets and found a total of 492 UPR-specific GBF2-bound genes, which significantly overlapped with UPR-specific bound genes of either bZIP28, bZIP60 or both bZIP28 and bZIP60 (Fig. 2e). Those co-bound genes showed strong enrichment of ER stress-related pathways (Fig. 2f and Supplementary Data 7), suggesting that GBF2, bZIP28 and bZIP60 co-regulate a set of genome-wide UPR genes at 0 h of ERR. Based on these results, we sought mechanistic insights

into the functional role of GBF2 in UPR gene expression using the *BiP3* promoter. At 0 h of ERR where the *BiP3* expression was exponentially induced as a hallmark of UPR activation[4,12] (Fig. 2g), GBF2, bZIP28 and bZIP60 co-bound the genomic locus of the *BiP3* promoter containing G-boxes, which overlapped with the DNase hypersensitive site (DHS)[29], a proxy of open chromatin (Fig. 2g), suggesting that these bZIP TFs control the expression of *BiP3* in concert. The *in vivo* binding of GBF2 to the *BiP3* promoter, which confirms the binding in yeast (Fig. 1f), was temporally regulated since it diminished at 12 h and 24 h of ER stress recovery (Extended Data Fig. 9). Consistent with the temporal binding of GBF2, the transcripts of *BiP3* were significantly induced in *gbf2-3* specifically at 0 h relative to Col-0 (Fig. 2h). Conversely, overexpression of *GBF2* in *GBF2ox* significantly reduced the expression of *BiP3* compared to Col-0 (Fig. 2i). Collectively, these results indicate that GBF2 functions as a gene repressor in the UPR, consistent with its interaction with HY5 in UPR regulation[27]. These results also support the hypothesis that GBF2 competes with bZIP28 and/or bZIP60 for binding to UPR gene promoters. To test this further, we used recombinant, purified, full-length GBF2, nucleus-imported form of bZIP28 (bZIP28n) and spliced form of bZIP60 (sbZIP60) proteins in electrophoretic mobility shift assays (EMSAs). GBF2 bound competitively and specifically the promoter fragment of *BiP3* (EW) containing the G-box (Fig. 3a,b), in accordance with our binding results in yeast (Fig. 1f) and plants (Fig. 2g and Extended Data Fig. 9). The GBF2-binding signal, which appeared saturated with the lowest protein mass (lane 3), depended on the intact G-box since GBF2 bound neither the promoter fragment containing a mutated G-box (EM; lane 13) or no G-box (EN; lane 14). Notably, adding bZIP28n (lane 9 and 10) or sbZIP60 (Lane 11 and 12) to the GBF2-binding reactions repressed and eventually removed the GBF2 binding to the EW with a dominant effect of sbZIP60, indicating that the DNA-binding activity of GBF2 was negatively affected by the presence of either

bZIP28n or sbZIP60. Then we asked if GBF2 could alter the DNA-binding activity of sbZIP60 (Fig. 3c). While sbZIP60 bound the *BiP3* promoter specifically via the G-box (competitive to unlabeled EW; no binding to EW or EM), adding GBF2 remarkably inhibited the G-box-specific binding of sbZIP60, albeit at a lesser extent compared to the effect of sbZIP60 on GBF2-binding to DNA. Intriguingly, we noted that sbZIP60-binding to the *BiP3* promoter was also repressed by bZIP28. Thus, our data demonstrate a competitive binding of GBF2 and bZIP60, or to a lesser extent bZIP28, to the *BiP3* promoter specifically via the G-box. To investigate the effects of the competitive binding of GBF2 and UPR-bZIP TFs on the expression of *BiP3 in planta*, we performed transient expression assays in agroinfiltrated tobacco leaves[30] using the Dual-Luciferase (LUC) Assay system[31] (Fig. 3d-e). While the normalized activity of LUC driven by the ~1-kb *BiP3* promoter containing the G-box and ERSE-I was increased by the addition of sbZIP60 effector cells (OD_{600} = 0.1) by 2.5 times (lane 2) relative to the one without any effector (lane 1), the induction was substantially enhanced by adding bZIP28n effector cells along with sbZIP60 (OD_{600} = 0.1 for each, totaling 0.2 of both effectors) (lane 3), suggesting that the UPR-bZIP TFs activate the *BiP3* expression in concert, in agreement with previous studies[4,11,12,22,23]. The increased activity of LUC by the addition of both UPR-bZIP TFs was dramatically suppressed when an equal density of GBF2 effector cells (OD_{600} = 0.2) was added (lane 5). Interestingly, the half density of GBF2 effector cells (OD_{600} = 0.1) had no significant effect on the increased activity of LUC by both UPR-bZIP TFs (lane 4), indicating a quantitative reaction for the competition. Collectively, our *in planta* data confirmed the competitive binding of GBF2 to the *BiP3* promoter observed *in vitro* (Fig. 3b,c) and further validated a UPR gene regulatory role of GBF2.

Based on these results and the evidence that the loss of *GBF2* enhances UPR gene responsiveness (Fig. 2h) and growth resilience in ER stress resolution (Fig. 2a,b), we hypothesized

that a *GBF2* null mutation would suppress the lethality of a *bzip28-2 bzip60-1* mutant[32] in both ERR and chronic ER stress during which pro-death processes are actuated, a similar phenotype of analogous mutants of mTF combinations in metazoan UPR[12,32]. We therefore generated a *gbf2-3 bzip28-2 bzip60-1* triple mutant and evaluated its sensitivity to ER stress relative to Col-0, *gbf2-3* and *bzip28-2 bzip60-1*. In ERR conditions (Fig. 4a), we found that the relative rate of *gbf2-3* recovery was higher than Col-0, consistent with our earlier experiments (Fig. 2a,b), but also that the lethal phenotype of *bzip28-2 bzip60-1* was partially suppressed by *gbf2-3*. The suppressive effect of *gbf2-3* in *bzip28-2 bzip60-1* was even stronger in chronic ER stress assays (i.e., direct seed germination and growth on Tm-containing culture media) (Fig. 4b). Our gene expression analyses here and previous studies showed that *BiP3* and another UPR biomarker gene, *ER-resident J protein 3B (ERdj3B)* which was also co-bound by GBF2, bZIP28 and bZIP60 (Supplementary Data 6), were not transcriptionally induced in *bzip28-2 bzip60-1* in Tm-treated condition compared to the DMSO (Fig. 4c)[12,33]. However, the *gbf2-3* mutation in *bzip28-2 bzip60-1* led to a remarkably increased expression of *BiP3* and *Erdj3B* in Tm conditions. Because the expression of *BiP3* and *Erdj3B* was derepressed in *gbf2-3 bzip28-2 bzip60-1* compared to *bzip28-2 bzip60-1* specifically in Tm-conditions, our data indicate that in ER stress-treated *bzip28-2 bzip60-1* the expression of *BiP3* and *Erdj3B* is modulated by bZIP28- and bZIP60-independent mechanisms, possibly dependent on the UPR master regulator Inositol Requiring Enzyme 1, but also support the data that, by binding to the promoters of UPR genes, GBF2 suppresses their expression.

Dysregulated UPR is potentially lethal and wasteful of stress response resources. Our results support a model for UPR regulation whereby a repressive role of GBF2 on UPR gene expression monitors the UPR activation. In ER stress situations requiring activation of the UPR,

bZIP28 and bZIP60 compete with GBF2 in the binding to the G-box for the activation of UPR gene expression. Notably, the repressive role of GBF2 occurs in ER stress situations, but not ER stress relief situations requiring deactivation of the UPR. Therefore, GBF2 may function to monitor adequate timing and amplitude of UPR gene expression to manage ER stress resources, such as UPR effectors (e.g., chaperones and foldases) that are associated with significant biological processes[34] and whose expression levels need to be tightly controlled because of frequent demands over the life cycle. Additional experiments are needed to establish how GBF2 can sense the appropriate timing of the action to modulate gene expression in the UPR. The repressive role of GBF2 and G-box is likely to be conserved in other multicellular organisms due to the exclusive prevalence of G-box and G-class bZIP TF family in eukaryotes[35]. As shown here, a TF competition phenomenon, which appears universal in yeast[36], plants[37] and mammals[38], underpins the UPR. Our findings contribute to understand the mechanisms for UPR gene regulation plasticity and provide new insights for discovering therapeutic and agronomic targets linked to UPR dysregulation in human disease[38] and crop loss[39].

Methods

Plant material and growth. *A. thaliana* ecotype Columbia-0 (Col-0) was used as the wild-type control. The following mutants and transgenic lines, which are in Col-0 background, were used in this study: *bzip28-2* (SALK_132285), *bzip60-2* (SAIL_283_B03), *bzip28-2 bzip60-1* (SALK_132285 SALK_050203), *gbf2-1* (SALK_206654), *gbf2-2* (SALK_205706), *gbf2-3* (SALK_087916), n*f-yc2* (SALK_111422), *wrky8* (SALK_050194), *lbd3* (SAIL_659_D08), *anac092* (SALK_090154), *anac036* (SAIL_600_D02), *hb28* (SALK_096579), *erf11* (SALK_085781), *nac2* (SALK_037700), *rap2.6* (SALK_051006), *anac062*

(WiscDsLoxHs100_07A), *gbf1* (SALK_027691), *gbf3* (SALK_056627), *GBF2ox* (CS2104585) and *pGBF2*:*GBF2-Ypet* (CS71581). All T-DNA single and high-order mutants used in this study were confirmed to be homozygous before the analysis. Primers used for genotyping are presented in Table S3. Surface-sterilized seeds were plated on half-strength Linsmaier Skoog (LS) medium (Caisson Labs, Ontario, Canada) supplemented with 1% sucrose (Sigma-Aldrich, St. Louis, MO, USA), and 1.2% Agar (Acumedia, Lansing, MI, USA). Appropriate antibiotics was also added for the screening of transgenic lines. After stratification in the dark at 4 °C for 2 days, plates were transferred to a controlled growth chamber with 80 μmol m−2 s−1 under 16 h light:8 h dark with 22 °C.

RNA-seq data analysis. RNA-seq data for response to ABA treatment[13] and ER stress recovery[4] were downloaded from NCBI Gene Expression Omnibus (GSE80568 and GSE146723, respectively) and processed in the same analysis pipeline as described below. The quality of raw reads was accessed using FastQC (version 0.11.5). Raw reads were cleaned for quality and adapters with Cutadapt (version 1.8.1)[40] using a minimum base quality of 20 retaining reads with a minimum length of 30 nucleotides after trimming. Quality-filtered reads were aligned to the Col-0 reference genome (TAIR10) using Bowtie (version 2.2.4)[41] and TopHat (version 2.0.14)[42] with a 10-bp minimum intron length and 15,000-bp maximum intron length. Per-gene read counts were measured using HTSeq (version 0.6.1p1)[43] in the union mode with a minimum mapping quality of 20 with stranded=reverse counting. Differential gene expression analysis was performed in each sample relative to the mock control using DESeq2 (version 1.16.1)[44] within R (version 4.1.2). Genes of which the total count is < 60 (ABA dataset, which has 2 biological replicates) or 100 (ER stress recovery dataset, which has 3 biological replicates) were not included in the analysis. DEGs

were obtained based on adjusted P-value < 0.01 and absolute Log_2FC > 1. For visualization purposes, tdf files of each replicate file were generated using igv tools (version 2.3.26) with the command "count" and loaded to Integrative Genome Browser (version 2.5.0)[45]. GO enrichment analysis was performed using clusterProfiler (version 4.2.2) and visualized using enrichplot (version 1.14.2) in R (version 4.1.2)[46].

ChIP assays, ChIP-qPCR, ChIP-seq library preparation. ChIP for GBF2 was performed using the same protocol applied to bZIP28 and bZIP60 ChIP analyses[4]. Plants germinated and were subjected to treatment with 500 ng/mL Tm or DMSO for 6 h, which is 0 h of ER stress recovery. Whole seedlings harvested in three biological replicates were completely submerged in freshly prepared crosslinking buffer (0.4 M Sucrose, 10 mM Tris-HCl, 1 mM EDTA, 1 mM PMSF, 1% Formaldehyde) in 50 mL conical tubes. Samples were subjected to a vacuum infiltration for 15 min and another for 5 min with glycine (125 mM final concentration). After the crosslinking buffer was removed, the crosslinked tissues were briefly rinsed with pre-chilled sterilized water, dried by gently blotting between paper towels, immediately frozen in the liquid nitrogen and stored at -80 °C for the next steps. The frozen tissues were ground to fine powder in liquid nitrogen using pre-chilled motors and pestles. After isolation, chromatin was fragmented using Covaris M220 sonicator (Covaris, Woburn, MA, USA) with settings of 3 cycles of PIP-50, duty factor 20% time-70s at 4 °C. Immunoprecipitation (IP) was performed with a polyclonal anti-GFP antibody ab290 (Abcam, Cambridge, UK) (1:200 dilution rate). For each ChIP sample, a mock (no antibody) and input (no IP) were included for control experiments. 2 µL of purified DNA (ChIP, mock and input), which was diluted by 4-fold, was used for quantitative PCR (qPCR) analysis in an ABI7500 machine (Applied Biosystems, Foster City, CA, USA) using Fast SYBR Green Master Mix (Life

Technologies, Carlsbad, CA, USA). Enrichment from ChIP DNA was first normalized relative to their input DNA. Three technical replicates were assayed for each of the three biological replicates. The list of primers used in ChIP-qPCR is provided in Supplementary Table 1. The final purified and ChIP and input DNAs were quantified using the Qubit fluorometer (Thermo Fisher Scientific, Carlsbad, CA, USA), and ChIP-seq libraries were constructed in two biological replicates using the NEBNext Ultra II DNA Library Prep Kit (New England BioLabs, Beverly, MA, USA) according to manufacturer's protocol. The suitable size distribution of libraries was confirmed using the 2100 Bioanalyzer (Agilent, Santa Clara, CA, USA). Multiplexed libraries of two biological replicates were sequenced in single-end mode on the Illumina NovaSeq 6000 platform (100-nt) at the Research Technology Support Facility Genomics Core at Michigan State University.

ChIP-seq data analysis. The quality of raw ChIP-seq reads was evaluated using FastQC (version 0.11.5). Reads were cleaned for quality and adapters with Cutadapt (version 1.8.1)[40] using a minimum base quality of 20 retaining reads with a minimum length of 30 nucleotides after trimming. Quality-filtered reads were aligned to the Col-0 reference genome (TAIR10) using Bowtie (version 1.1.2)[47] with parameters "-n 2 -m 3 -k 1 –threads 7 –best –chunkmbs 256 -q". Duplicated reads were removed using Samtools (version 1.8)[48]. Peak calling was performed using MACS2 (version 2.1.2)[49] in individual samples with the corresponding input samples with a relaxed threshold of P-value (--pvalue=1e-2), as recommended by the IDR pipeline (https://sites.google.com/site/anshulkundaje/projects/idr). Peaks across replicates with an IDR < 0.10 for GBF2 or < 0.5 for bZIP28 and bZIP60 were retained for further analysis. To obtain UPR-specific binding peaks with high-confidence, we applied two parameters to IDR-filtered peaks; (1)

a peak called in Tm samples that was overlapped with a peak in the corresponding DMSO-treated samples by > 30% was eliminated, (2) Among the peaks that were overlapped with peaks in DMSO-treated sample, if its *P* float (8th column in the IDR output file) in the Tm-treated sample was higher than the corresponding peak in the DMSO-treated sample by greater than 3-fold, the peak was retained and named as a UPR-specific binding peak. UPR-specific binding peaks obtained at each time-point were merged into a single list for further analysis and were annotated using the ChIPseeker (version 1.30.3) and the GenomicFeatures R Package (version 4.1.2)[50]. For visualization purposes, bigwig files (using pooled data across biological replicates) were generated by the deepTools suite (https://deeptools.readthedocs.io/en/develop/)[51] (version 2.0) with the command "bamCoverage"; read coverage was normalized as CPM (Counts Per Million mapped reads). ChIP-seq tracks were visualized in Integrative Genome Browser (version 2.9.2)[45]. UPR-specific binding peaks were mapped to the vicinity of a transcript sequence (< 3-kb upstream or downstream), generating a total of 492 GBF2-, 105 bZIP28- and 217 bZIP60-bound genes, respectively. GO enrichment analysis was performed using clusterProfiler (version 4.2.2) and visualized using enrichplot (version 1.14.2) in R (version 4.1.2)[46].

Cistrome analysis. The cistrome analysis was performed on overlapping 110-bp fragment spanning the 1-kb upstream sequences of the transcription start site, hereafter called 1-kb promoter, in the TAIR10 annotation, using tools of MEME suite (version 5.0.5) (http://meme-suite.org) with default parameters and modifications indicated below. Among the 928 DEGs that were responsive to both ABA treatment and ER stress recovery, 1-kb promoters of 922 DEG were obtained from the BioMart tool at the Phytozome database (version 13; https://phytozome-next.jgi.doe.gov) and used in the analysis since the promoter sequences of the six genes were not available in TAIR10.

As a control set, 922 genes were randomly selected and the 1-kb promoter sequences of the random genes were obtained as described above. Each 1-kb promoter of 922 DEGs and random 922 genes was split into 10 fragments (-1000-bp to -890-bp; -900-bp to -790-bp; - 800-bp to -690-bp; -700-bp to -590-bp; -600-bp to -490-bp; -500-bp to -390-bp; -400-bp to -290-bp; -300 to -190; -200-bp to -90; - 100 to -1-bp) using seqtk (version 1.3). *De novo* motif discovery in each promoter fragment set of the DEGs was performed using STREME[52] with a parameter of "–minw 5 –maxw 25 –pvt 0.05" with the control set of random genes. The similarity of enriched motifs with DNA affinity purification sequencing motifs[53] and protein-binding microarray motifs[54] was assessed using TOMTOM[55].

Promoter cloning, yeast transformation and eY1H. The genomic DNA of Col-0 was extracted from two-week-old seedlings using the DNasesy Plant Mini Kit (Qiagen, Valencia, CA, USA) and used for subsequent promoter cloning in this study. Promoter fragments, as described in Fig. 1d, were amplified from the genomic DNA using Phusion High-Fidelity DNA Polymerase (New England BioLabs, Beverly, MA, USA). Promoter fragments were recombined either into pDONR P4-P1R using BP clonase II or pENTR 5'-TOPO (Supplementary Table 1) (Life Technologies, Grand Island, NY, USA) to create entry clones. The resulting entry clones were sequence-confirmed and then recombined into both pMW2 and pMW3 using LR clonase II (Life Technologies, Grand Island, NY, USA). The resulting pMW2 and pMW3 constructs were sequence-confirmed and then transformed into the yeast strain YM4271, as previously described[56]. Yeast colonies were screened for autoactivation and construct presence. Promoter strains were mated against a collection of > 2000 Arabidopsis TF strains[57] using a Singer Instruments ROTOR HDA robot platform in the Yeast One Hybrid Services Core at the Genome Center at the University

of California Davis, as previously described[20,21,58]. The list of primers used in the promoter amplification is provided in Supplementary Table 2.

Visualization of TF network. The TF network (Fig. 1f) was visualized using Cytoscape (version 3.8.2)[59]. A text file was compiled to include all PDIs (TF to gene) and the corresponding gene expression data (log_2-transformed expression fold-change) at 0, 12, and 24 h of ERR. The file was used as an input file in which a row corresponded to an interaction between source and target. The yFiles Organic Layout was applied to the network visualization. The selected TFs and bait genes were manually labeled in the network. Gene ontology (GO) enrichment analysis was performed using agriGO (version 2.0) (http://systemsbiology.cau.edu.cn/agriGOv2/)[60] with a false-discovery rate adjusted $P < 0.05$ (hypergeometric test) as a cutoff.

ER stress and ABA treatment assays. For ERR assay, 5-day-old seedlings were transferred to half-strength LS liquid buffer containing either 0.5 µg/mL Tm (Sigma-Aldrich, St. Louis, MO, USA) or DMSO-only as mock, and incubated for 6 h. After the drug treatment, seedlings were transferred to 100x100 square Petri dishes with grid (Fisher Scientific, Hampton, NH, USA) containing half-strength LS medium (Caisson Labs, Ontario, Canada) supplemented with 1% sucrose (Sigma-Aldrich, St. Louis, MO, USA), 1.2% Agar (Acumedia, Lansing, MI, USA). Each square plate was split into two portions, of which each side accommodated either Tm-treated seedlings or DMSO-only-treated seedlings, and served as a biological replicate (n = 6 per replicate). Then, the seedlings grew vertically under the normal growth condition. To transiently induce the *GBF2* expression in *GBF2ox* during the recovery from ER stress, β-estradiol (Sigma-Aldrich, St. Louis, MO, USA) was added to the recovery growth media at a final concentration of

10 µM. For chronic ER stress assay, seeds were plated on half-strength LS medium (Caisson Labs, Ontario, Canada) supplemented with 1% sucrose (Sigma-Aldrich, St. Louis, MO, USA), 1.2% Agar (Acumedia, Lansing, MI, USA) and 25 ng/mL Tm (Sigma-Aldrich, St. Louis, MO, USA) or DMSO alone as mock. For measuring the primary root length of seedlings, plates were photo-scanned at the same of time of the day. The length of primary roots was measured using ImageJ software (https://imagej.nih.gov). For the ABA treatment assay, 5-day-old seedlings were transferred to half-strength LS liquid buffer containing 3 µM ABA (Sigma-Aldrich, St. Louis, MO, USA) or EtOH-only as mock, incubated, and harvested at 1, 4 and 24 h after the incubation. All experiments were independently replicated with consistent results.

RNA extraction and qRT-PCR analysis. Plants germinated and were subjected to the ER stress recovery or ABA treatment assays as described above. Whole seedlings were harvested at 0 h, 12 h and 24 h of ER stress recovery in three biological replicates (n = 12 per each replicate), except for *GBF2ox* seedlings which were harvested only at 24 h to sufficiently induce the *GBF2* expression, and immediately frozen in the liquid nitrogen. The frozen samples were ground to a fine powder in liquid nitrogen using a Retch MM400 Mixer Mill with zirconium oxide balls. Total RNA was extracted using the NucleoSpin RNA Plant kit (MACHEREY-NAGEL, Düren, Germany) according to the manufacturer's instruction. cDNA was synthesized from 1 µg of DnaseI-treated total RNA using iScript cDNA Synthesis Kit (BIO-RAD, Hercules, CA, USA) according to the manufacturer's instruction. For qRT-PCR, Fast SYBR Green Master Mix (Applied Biosystems, Foster City, CA, USA) was used in the presence of gene-specific primers and template cDNAs in an ABI7500 (Applied Biosystems, Foster City, CA, USA). The list of primers used in qRT-PCR is provided in Supplementary Table 2.

Vector construction and purification of recombinant bZIP28, bZIP60 and GBF2 proteins. The coding sequence (CDS) of bZIP28n, sbZIP60 and GBF2 were amplified from Col-0 cDNA using Phusion High-Fidelity DNA Polymerase (New England BioLabs, Beverly, MA, USA) with primers tailed with restriction enzyme sites: NcoI (forward) and BamHI (reverse) for bZIP28n and sbZIP60; SalI (forward) and EcoRI (reverse) for GBF2. The bZIP28n, sbZIP60 and GBF2 cDNA fragments were cloned into pGEM-T (Promega, Madison, Wisconsin), generating bZIP28n-T, sbZIP60-T and GBF2-T constructs. After sequence verification, the bZIP28n, sbZIP60 and GBF2 cDNA CDSs were subcloned into pMAL-c5X (New England BioLabs, Beverly, MA) through the corresponding restriction enzyme sites. E. coli strain BL21 competent cells were used to transform empty pMAL (expressing the only maltose-binding protein, MBP), pMAL-bZIP28n, pMAL-sbZIP60 or pMAL-GBF2, which were grown in 4 ml of Luria-Bertani (LB) media with Carbenicillin (100 mg/L) at 37 °C for 18 h. The overnight cultures of BL21 cells containing pMAL, pMAL-bZIP28n, pMAL-sbZIP60 or pMAL-GBF2 construct were diluted into 1:100 in 80 mL LB media with Carbinicillin (100 mg/L) and grown at 37 °C to an OD600 value of 0.5, when isopropyl-β-D-thiogalactoside (IPTG) (0.1 mM) was added. After 20 h of additional incubation at 16 °C, cells were harvested after centrifugation at 4,000 g at 4 °C for 10 min and resuspended in 2 mL of Column buffer (20 mM Tris-HCl, 200 mM NaCl, 1 mM EDTA). After frozen at -20 °C for 18 h, cells were lysed by a Sonicator (Virtis, Gardiner, NY) and centrifuged at 20,000 g at 4 °C for 20 min. The cleared cell lysates were diluted 1:5 with Column buffer, and loaded on amylose-coupled agarose resin columns prepared according to the manufacturer's instruction (New England BioLabs, Beverly, MA). After columns were washed with 12 volumes of Column buffer, MBP, MBP-bZIP28n, MBP-sbZIP60 and MBP-GBF2 were eluted with elution buffer (20

413 mM Tris-HCl, 200 mM NaCl, 1 mM EDTA, 10 mM Maltose). After filtration by Amicon Ultra
414 30 K (Millipore, Darmstadt, Germany), the purified MBP, MBP-bZIP28n, MBP-sbZIP60 and
415 MBP-GBF2 were aliquoted and stored at -80 °C. The list of primers used in the cloning is provided
416 in Extended Data Table 2.

417

418 **EMSA**. PAGE-purified sense and antisense oligonucleotides were annealed in an annealing buffer
419 (300 mM KCl, 30 mM HEPES-pH 7.5 and 1.0 mM MgCl2) at 94 °C for 2 min and gradually
420 cooled to create double-stranded DNA probes (EW, EM and EN). The double-stranded
421 oligonucleotides were [^{32}P] end-labeled using a T4 Polynucleotide Kinase according to the
422 manufacturer's instruction (New England BioLabs, Beverly, MA). The recombinant proteins (10
423 to 30 pmol) were mixed with 40 fmol of the radiolabeled probes, without or with variable amounts
424 of unlabeled competitor DNA in reaction buffer (25 mM HEPES-KOH pH7.5, 2.5 mM DTT, 75
425 mM KCl, 10% glycerol, 1.25 ng poly-dIdC). Each reaction was incubated at room temperature for
426 10 min without the probes and then incubated on ice for 20 min with the radiolabeled probes. The
427 competitor concentrations were at 0.01, 0.05 and 0.1 pmol. After the incubation, the reaction
428 mixtures were resolved by electrophoresis on a 5% non-denaturing polyacrylamide gel. Gels were
429 dried in a gel dryer (Hoefer, Holliston, MA) and exposed to X-ray film (Kodak, Rochester, NY).
430 The list of oligo probes used in EMSA is provided in Extended Data Table 2.

431

432 **Vector construction for Dual-Luciferase Assay**. For the reporter construct, the promoter
433 fragment (-1000-bp to +37-bp) of *BiP3* was amplified from Col-0 genomic DNA using Phusion
434 High-Fidelity DNA Polymerase (New England BioLabs, Beverly, MA, USA) with primers tailed
435 with restriction enzyme sites: BamHI (forward) and NcoI (reverse). The BiP3 promoter fragment

was cloned into pGEM-T (Promega, Madison, Wisconsin). After sequence verification, it was subcloned into pGreenII 0800-LUC through restriction enzyme sites, BamHI (forward) and NcoI (reverse), generating the *BiP3* promoter reporter construct. For effector constructs, the CDS of *bZIP28n*, *sbZIP60* and *GBF2* cloned in bZIP28n-T, sbZIP60-T and GBF2-T plasmids, respectively, were subcloned into pGreenII 62-SK through restriction enzyme sites: NcoI (forward) and BamHI (reverse) for bZIP28n and sbZIP60; SacII (forward) and EcoRI (reverse) for GBF2. The reporter and effector plasmids were introduced into *Agrobacterium tumefaciens* strain GV3101 along with pSOUP. The transformed cells were plated on LB agar media with rifampicin (25 µg/mL), kanamycin (50 µg/mL), and gentamicin (100 µg/mL).

Dual-Luciferase Assay. One single colony of *A. tumefaciens* cells transformed with either the reporter (*BiP3*:*LUC*) or one of the effectors (*35Spro*:*sbZIP60*, *35Spro*:*bZIP28n* and *35Spro*:*GBF2*) was inoculated in 5 mL LB media with kanamycin (50 µg/mL), and gentamicin (100 µg/mL) at 28 °C overnight. 1 mL of the overnight culture was inoculated in 25 mL LB media with kanamycin (50 µg/mL), and gentamicin (100 µg/mL) at 28 °C overnight. The overnight culture was centrifuged at 1,500 x g for 10 min and the pellet was resuspended in 10 mL Resuspension Solution (10 mM MgCl2 and 10 mM MES-K pH 5.6). The centrifugation step was repeated to remove traces of antibiotics. *A. tumefaciens* cell cultures transformed with each of the constructs were mixed and adjusted to have 0.1 of the final OD_{600} according to the experiment strategy. After being incubated in the dark at room temperature for 24 h before infiltration, the cell suspension was infiltrated into the abaxial surface of 4-weeks-old tobacco leaves using disposable 1 mL syringes. After growth for 72 h, 1 cm leaf discs (one disc for each replicate) were harvested, snap-frozen, and ground to a fine powder in liquid nitrogen using a Retch MM400 Mixer Mill with zirconium

oxide balls. Ground tissue powder of each leaf disc was homogenized with 300 µL of the Passive Lysis Buffer (PLB) provided in the Dual-Luciferase Assay kit (Promega, Madison, Wisconsin). Homogenized samples were centrifuged at 7,500 x g for 1 min. The supernatant was diluted 5-fold in PLB and ready for the assay. 15 µL of each sample was loaded into a well of Nun F96 MicroWell White Polystyrene Plate (Thermo Fisher Scientific, Waltham, MA). The plate was loaded into the GloxMax Navigator luminometer (Promega, Madison, Wisconsin). The dual injectors were used to dispense 75 µL of luciferase assay reagent and Stop & Glo reagent into each well, respectively. The relative activity of luciferase was normalized by the intensity of the internal control, *Renilla*. Each biological replicate was measured in 3 technical replicates.

Statistical analyses. Statistical calculations were conducted using R (version 4.1.2) and Microsoft Excel. Statistical analyses were performed using a two-tailed Student *t*-test and hypergeometric probability test. The exact sample sizes (n) and all raw data for each experimental group/condition are given as discrete numbers in each figure panel. Additional information is available in the Reporting Summary, which includes statements on statistics, software used and data availability and Source data.

Reporting Summary

Further information on research design is available in the Nature Research Reporting Summary linked to this article.

Data availability

All data supporting the findings of this study are available within this paper and its Supplementary Materials files. The ChIP-seq data supporting the finding of this study have been deposited in the NCBI Sequence Read Archive and are accessible through the BioProject accession code PRJNA810750. The full results of the eY1H screen, including gene accession numbers, are available in Supplementary Data 4. The source data are provided with this paper.

Code availability

The scripts used in this study are available in GitHub (https://github.com/DaeKwan-Ko/UPR-TFs.git).

Acknowledgments

This study was supported primarily by the National Institutes of Health (R35GM136637) with contributing support from by the Great Lakes Bioenergy Research Center, U.S. Department of Energy, Office of Science, Office of Biological and Environmental Research (DE-SC0018409), Chemical Sciences, Geoscience and Biosciences Division, Office of Basic Energy Sciences, Office of Science, U.S. Department of Energy (DE-FG02-91ER20021) and MSU AgBioResearch (MICL02598). This study was supported in part through Michigan State University's Institute for Cyber-Enabled Research Cloud Computing Fellowship, with computational resources and services provided by Information Technology Services and the Office of Research and Innovation at Michigan State University. We thank the Genome Center and Proteomics Core, University of California, Davis for the eY1H screen.

Author Contributions

D.K.K and F.B. conceived the project and designed experiments and research plan; D.K.K performed experiments and data analysis; F.B. supervised the project; D.K.K and F.B. interpreted the data and wrote the manuscript.

Competing interests

The authors declare no conflicts of interest.

Figure Legends

Fig. 1 | Putative CRE identification relevant to differential gene expression in response to both ABA treatment and ER stress recovery and a UPR-TF network built on Y1H screens. **a**, RNA-seq results in ABA treatment and ERR condition show a significant overlap of DEGs. The significance (*P*-value) measured by one-sided hypergeometric distribution test is shown. **b**, Pairwise correlation analyses of relative expression levels of DEGs between ABA-36 h and ERR conditions. The expression of each of the DEGs (36 h of ABA treatment and 0 h, 12 h or 24 h of ERR; n = 105 for ABA-36 h vs. ERR-0 h, n = 277 for ABA-36 h vs. ERR-12 h, n = 315 for ABA-36 h vs. ERR-24 h) were subjected to Spearman correlation coefficient analyses. n = the number shared DEGs. The density plots at the top and right display the enrichment of Log_2FC under ER stress recovery and ABA (36 h), respectively. The Spearman's correlation coefficient (rho) for each comparison is shown along with the level of significance (*P*-value) in the corresponding color. Plots of the other ABA time-points are shown in Extended Data Fig. 2. Error bars (gray) denote 95% confidence intervals. **c**, *De novo* motif analyses of promoter fragments of the ERR-ABA DEGs with STREME. The 1-kb promoters of each of the ERR-ABA DEGs were split into 10 overlapping fragments (110-bp long except for the ones closest to TSSs, which are 100-bp) and

subjected to *de novo* motif analyses with a control set of randomly selected genes (See Methods and Extended Data Fig. 3). STREME used Fisher's exact test to calculate *P*-values of each motif enrichment. Full information of TOMTOM results is provided in Supplementary Data 3. **d**, A schematic view of the 1-kb promoters of *bZP28*, *bZIP60* and *BiP3* genes used for bait in the eY1H screens. Coordinates of each fragment bait are indicated. Fa, fragment a (away from the transcription start site). Fb, fragment b (containing the transcription start site). **e**, Distribution of TF interaction hits for each promoter fragment (Fa or Fb) of each bait gene. **f**, A TF network underlying the UPR. Square nodes indicate individual TFs. Bait genes (*bZIP28*, *bZIP60* and *BiP3*) are shown as black circles. Three horizontal strip heatmaps within each node indicate expression changes in Col-0 during ER stress recovery (0 h, 12 h and 24 h). A full list of PDIs identified in our Y1H screens is provided in Supplementary Data 4.

Fig. 2 | GBF2 negatively regulates the expression of *BiP3* via direct binding to the promoter. **a,b**, A heatmap (**a**) showing the relative growth rate of the primary roots of T-DNA mutants of selected 12 TF genes. The relative growth rate of primary roots was measured at Day 7 in ERR. Representative images (**b**) of the primary root of Col-0 and *gbf2-3* are shown. **c**, Genomic annotations of GBF2 UPR-specific binding peaks. A full list of peak annotation is provided in Supplementary Data 6. d, Top-scoring motif (G-box) enriched in centers of GBF2 Tm-specific binding peaks. e, Intersection of GBF2 UPR-specific binding peaks with those of UPR bZIP-TFs. The *P*-values of the overlaps between the two datasets or among multi-sets measured using one-sided hypergeometric distribution test are shown. The degree of intersection is indicated in the heatmap above the plot. The genes indicated by red dashed lines were used for the GO term enrichment analysis in (**f**). **f**, GO term enrichments in genes bound by GBF2 and UPR mTF(s). The 13 GO terms with the largest gene ratios are plotted in order of gene ratio. The *P*-values were

calculated by hypergeometric probability test and adjusted by the Benjamini-Hochberg method. The size of the dots represents the number of genes in the significant DE gene list associated with the GO term and the color of the dots represent the adjusted *P*-values. A full list of GO terms is provided in Supplementary Data 6. **g**, Genome browser screenshots visualizing GBF2, bZIP28 and bZIP60 binding to the promoter of *BiP3* and its expression at ERR-0 h. Arrows indicate gene orientation. DHS, DNase I hypersensitive sites. All tracks were normalized to the respective sequencing depth. The UPR-specific peak for each of GBF2, bZIP28 or bZIP60 is indicated by blue sold lines below the corresponding ChIP track. **h**, qRT-PCR assays of *BiP3* expression (Log_2[Tm/DMSO]) during ERR (0 h, 12 h and 24 h). Means ± SEM; n = 3 biological replicates (12 seedlings per replicate) except for Tm at 24 h where two biological replicates were used. The significance (*P*-value) measured by two-tailed Student's *t*-test is shown. **i**, qRT-PCR assays of *GBF2* and *BiP3* expression in the GBF2 β-estradiol inducible line. The expression values were calculated relative to *UBQ10*. Means ± SEM; n = 3 biological replicates (12 seedlings per replicate). D, DMSO; T, Tunicamycin; BE, β-estradiol. The significance (*P*-value) measured by two-tailed Student's *t*-test is shown. The experiments in **a**,**b**,**h**,**i** were independently repeated at least two times with similar results.

Fig. 3 | GBF2 competes with bZIP60 and bZIP28 for the binding to the *BiP3* promoter as a negative regulator. a, A schematic view of the 1-kb promoter of *BiP3*. Locations of G-box and ERSE-I are indicated by red and blue arrowheads, respectively. The grey bars indicate the location of probes (EW, EM and EN) used in the EMSA. Numbers are relative to the transcription start site (+1). **b**,**c**, EMSA of *BiP3* promoter probes with recombinant MBP-GBF2 (**b**) and MBP-sbZIP60 (**c**) (10, 20 and 30 pmole for lane 3, lane 4 and lane 5 through 14). Radioisotope-labeled probes (EW, EM and EN) were incubated in the presence of MBP, MBP-bZIP28n, MBP-sbZIP60 and

MBP-GBF2. Unlabeled EW probes (0.5×, 2.5× and 5× molar excess relative to labeled EW) were used as competitors. MBP-bZIP28n and MBP-sbZIP60 were used as competitors for MBP-GBF2 while MBP-bZIP28n and MBP-GBF2 were so for MBP-sbZIP60 (1.5 pmole for lanes 9 and 11, and 3 pmole for lanes 10 and 12). Shifted protein-DNA complexes are indicated by a black arrowhead. Free probes were indicated by a grey arrowhead. EW: the endogenous promoter fragment containing G-box and ERSE-I. EM: EW containing mutations on the G-box (gacGc). EN: the endogenous promoter fragment with no G-box or ERSE-I. **d**, Schematic diagram shows the constructs used in Dual-Luciferase Assays. BiP3pro, the *BiP3* promoter (1,037-bp). 35Spro, the CaMV 35S promoter. **e**, Dual-Luciferase Assays in tobacco leaves. Each plus sign indicates the addition of the corresponding *Agrobacterium* cell culture with 0.1 of OD_{600}, and two plus signs do so with 0.2 of OD_{600}. Data were normalized to the internal control REN, *Renilla*. Means ± SEM; $n = 5$ biological replicates (3 seedlings per replicate). The significance (*P*-value) measured by two-tailed Student's *t*-test is shown. ns, not significant. The experiments were independently repeated at least two times with similar results.

Fig. 4 | The *gbf2-3* null mutation suppresses the lethal phenotype of *bzip28-2 bzip60-1* and de-represses the expression of UPR biomarker genes. a,b, The relative growth of primary roots of Col-0, *gbf2-3*, *bzip28-2 bzip60-1* and *gbf2-3 bzip28-2 bzip60-1* in ERR (**a**) and chronic ER stress (**b**). The relative length of primary root was measured at 7 days of ER stress recovery and 10 days of growth under chronic ER stress. Means ± SEM; 5 biological replicates ($n = 6$ seedlings per replicates). (**c**) qRT-PCR assays of *BiP3* and *ERdj3B* expression in Col-0, *bzip28-2 bzip60-1* and *gfb2-3 bzip28-2 bzip60-1* after treatment with either Tm or DMSO for 6 h. The expression values were calculated relative to *UBQ10*. Means ± SEM; 5 biological replicates ($n = 12$ seedlings per

replicates). The significance (*P*-value) measured by two-tailed Student's *t*-test is shown. ns, not significant. The experiments were independently repeated at least two times with similar results.

References

1. Howell, S.H. Endoplasmic reticulum stress responses in plants. *Annu Rev Plant Biol* **64**, 477-99 (2013).
2. Pastor-Cantizano, N., Ko, D.K., Angelos, E., Pu, Y. & Brandizzi, F. Functional Diversification of ER Stress Responses in Arabidopsis. *Trends Biochem Sci* **45**, 123-136 (2020).
3. Ko, D.K. & Brandizzi, F. A temporal hierarchy underpins the transcription factor-DNA interactome of the maize UPR. *Plant J.* **105**(2020).
4. Ko, D.K. & Brandizzi, F. Advanced genomics identifies growth effectors for proteotoxic ER stress recovery in Arabidopsis thaliana. *Commun Biol.* **5**(2022).
5. Vihervaara, A., Duarte, F.M. & Lis, J.T. Molecular mechanisms driving transcriptional stress responses. *Nat Rev Genet.* **19**, 385-397 (2018).
6. Lemon, B. & Tjian, R. Orchestrated response: a symphony of transcription factors for gene control. *Genes Dev* **14**, 2551-69 (2000).
7. Ezer, D. *et al.* The G-Box Transcriptional Regulatory Code in Arabidopsis. *Plant Physiol.* **175**, 628-640 (2017).

8. Komili, S. & Silver, P.A. Coupling and coordination in gene expression processes: a systems biology view. *Nat Rev Genet* **9**, 38-48 (2008).
9. Ko, D.K. & Brandizzi, F. Network-based approaches for understanding gene regulation and function in plants. *Plant J.* (2020).
10. Martínez, I.M. & Chrispeels, M.J. Genomic analysis of the unfolded protein response in Arabidopsis shows its connection to important cellular processes. *Plant Cell* **15**, 561-76 (2003).
11. Liu, J.X. & Howell, S.H. bZIP28 and NF-Y transcription factors are activated by ER stress and assemble into a transcriptional complex to regulate stress response genes in Arabidopsis. *Plant Cell* **22**, 782-96 (2010).
12. Ruberti, C., Lai, Y. & Brandizzi, F. Recovery from temporary endoplasmic reticulum stress in plants relies on the tissue-specific and largely independent roles of bZIP28 and bZIP60, as well as an antagonizing function of BAX-Inhibitor 1 upon the pro-adaptive signaling mediated by bZIP28. *Plant J* **93**, 155-165 (2018).
13. Song, L. *et al.* A transcription factor hierarchy defines an environmental stress response network. *Science* **354**(2016).
14. Vihervaara, A., Duarte, F.M. & Lis, J.T. Molecular mechanisms driving transcriptional stress responses. *Nat Rev Genet* **19**, 385-397 (2018).
15. Lai, Y.S. *et al.* Salicylic acid-independent role of NPR1 is required for protection from proteotoxic stress in the plant endoplasmic reticulum. *Proc Natl Acad Sci U S A* **115**, E5203-E5212 (2018).
16. Nawkar, G.M. *et al.* HY5, a positive regulator of light signaling, negatively controls the unfolded protein response in. *Proc Natl Acad Sci U S A* **114**, 2084-2089 (2017).

17. Zhang, S.S. *et al.* Tissue-Specific Transcriptomics Reveals an Important Role of the Unfolded Protein Response in Maintaining Fertility upon Heat Stress in Arabidopsis. *Plant Cell* **29**, 1007-1023 (2017).
18. Zou, C. *et al.* Cis-regulatory code of stress-responsive transcription in Arabidopsis thaliana. *Proceedings of the National Academy of Sciences* **108**, 14992-14997 (2011).
19. Jakoby, M. *et al.* bZIP transcription factors in Arabidopsis. *Trends Plant Sci* **7**, 106-11 (2002).
20. Gaudinier, A. *et al.* Enhanced Y1H assays for Arabidopsis. *Nat Methods* **8**, 1053-5 (2011).
21. Reece-Hoyes, J.S. *et al.* Enhanced yeast one-hybrid assays for high-throughput gene-centered regulatory network mapping. *Nat Methods* **8**, 1059-64 (2011).
22. Deng, Y. *et al.* Heat induces the splicing by IRE1 of a mRNA encoding a transcription factor involved in the unfolded protein response in Arabidopsis. *Proc Natl Acad Sci U S A* **108**, 7247-52 (2011).
23. Song, Z.T. *et al.* Transcription factor interaction with COMPASS-like complex regulates histone H3K4 trimethylation for specific gene expression in plants. *Proc Natl Acad Sci U S A* **112**, 2900-5 (2015).
24. Otero, J.H., Lizák, B. & Hendershot, L.M. Life and death of a BiP substrate. in *Seminars in cell & developmental biology* Vol. 21 472-478 (Elsevier, 2010).
25. Smit, M.E. *et al.* Specification and regulation of vascular tissue identity in the. *Development* (2020).

660 26. Schindler, U., Menkens, A.E., Beckmann, H., Ecker, J.R. & Cashmore, A.R.
661 Heterodimerization between light-regulated and ubiquitously expressed Arabidopsis GBF
662 bZIP proteins. *The EMBO journal* **11**, 1261-1273 (1992).
663 27. Kurihara, Y., Makita, Y., Shimohira, H. & Matsui, M. Time-Course Transcriptome Study
664 Reveals Mode of bZIP Transcription Factors on Light Exposure in. *Int J Mol Sci*
665 **21**(2020).
666 28. Yu, C.P., Lin, J.J. & Li, W.H. Positional distribution of transcription factor binding sites
667 in Arabidopsis thaliana. *Sci Rep* **6**, 25164 (2016).
668 29. Zhang, T., Marand, A.P. & Jiang, J. PlantDHS: a database for DNase I hypersensitive
669 sites in plants. *Nucleic Acids Res* **44**, D1148-53 (2016).
670 30. Sparkes, I.A., Runions, J., Kearns, A. & Hawes, C. Rapid, transient expression of
671 fluorescent fusion proteins in tobacco plants and generation of stably transformed plants.
672 *Nat Protoc* **1**, 2019-25 (2006).
673 31. Sherf, B.A., Navarro, S.L., Hannah, R.R. & Wood, K.V. Dual-luciferase reporter assay:
674 an advanced co-reporter technology integrating firefly and Renilla luciferase assays.
675 *Promega notes* **57**, 2-8 (1996).
676 32. Deng, Y., Srivastava, R. & Howell, S.H. Protein kinase and ribonuclease domains of
677 IRE1 confer stress tolerance, vegetative growth, and reproductive development in
678 Arabidopsis. *Proc Natl Acad Sci U S A* **110**, 19633-8 (2013).
679 33. Lai, Y.S. *et al.* Systemic signaling contributes to the unfolded protein response of the
680 plant endoplasmic reticulum. *Nat Commun* **9**, 3918 (2018).

34. Pobre, K.F.R., Poet, G.J. & Hendershot, L.M. The endoplasmic reticulum (ER) chaperone BiP is a master regulator of ER functions: Getting by with a little help from ERdj friends. *J Biol Chem* **294**, 2098-2108 (2019).
35. Deppmann, C.D. *et al.* Dimerization specificity of all 67 B-ZIP motifs in Arabidopsis thaliana: a comparison to Homo sapiens B-ZIP motifs. *Nucleic Acids Res* **32**, 3435-45 (2004).
36. Gordân, R. *et al.* Genomic regions flanking E-box binding sites influence DNA binding specificity of bHLH transcription factors through DNA shape. *Cell Rep* **3**, 1093-104 (2013).
37. Nuruzzaman, M., Sharoni, A.M. & Kikuchi, S. Roles of NAC transcription factors in the regulation of biotic and abiotic stress responses in plants. *Front Microbiol* **4**, 248 (2013).
38. Altman, B.J. *et al.* MYC Disrupts the Circadian Clock and Metabolism in Cancer Cells. *Cell Metab* **22**, 1009-19 (2015).
39. Li, Z., Tang, J., Srivastava, R., Bassham, D.C. & Howell, S.H. The Transcription Factor bZIP60 Links the Unfolded Protein Response to the Heat Stress Response in Maize. *Plant Cell* **32**, 3559-3575 (2020).
40. Martin, M. Cutadapt removes adapter sequences from high-throughput sequencing reads. *EMBnet. journal* **17**, 10-12 (2011).
41. Langmead, B. & Salzberg, S.L. Fast gapped-read alignment with Bowtie 2. *Nat Methods* **9**, 357-9 (2012).
42. Kim, D. *et al.* TopHat2: accurate alignment of transcriptomes in the presence of insertions, deletions and gene fusions. *Genome Biol* **14**, R36 (2013).

43. Anders, S., Pyl, P.T. & Huber, W. HTSeq--a Python framework to work with high-throughput sequencing data. *Bioinformatics* **31**, 166-9 (2015).
44. Love, M.I., Huber, W. & Anders, S. Moderated estimation of fold change and dispersion for RNA-seq data with DESeq2. *Genome Biol* **15**, 550 (2014).
45. Robinson, J.T. *et al.* Integrative genomics viewer. *Nat Biotechnol* **29**, 24-6 (2011).
46. Wu, T. *et al.* clusterProfiler 4.0: A universal enrichment tool for interpreting omics data. *Innovation (N Y)* **2**, 100141 (2021).
47. Langmead, B., Trapnell, C., Pop, M. & Salzberg, S.L. Ultrafast and memory-efficient alignment of short DNA sequences to the human genome. *Genome Biol* **10**, R25 (2009).
48. Li, H. *et al.* The Sequence Alignment/Map format and SAMtools. *Bioinformatics* **25**, 2078-9 (2009).
49. Zhang, Y. *et al.* Model-based analysis of ChIP-Seq (MACS). *Genome Biol* **9**, R137 (2008).
50. Yu, G., Wang, L.G. & He, Q.Y. ChIPseeker: an R/Bioconductor package for ChIP peak annotation, comparison and visualization. *Bioinformatics* **31**, 2382-3 (2015).
51. Ramírez, F. *et al.* deepTools2: a next generation web server for deep-sequencing data analysis. *Nucleic Acids Res* **44**, W160-5 (2016).
52. Bailey, T.L. STREME: Accurate and versatile sequence motif discovery. *Bioinformatics* (2021).
53. O'Malley, R.C. *et al.* Cistrome and Epicistrome Features Shape the Regulatory DNA Landscape. *Cell* **165**, 1280-1292 (2016).
54. Franco-Zorrilla, J.M. *et al.* DNA-binding specificities of plant transcription factors and their potential to define target genes. *Proc Natl Acad Sci U S A* **111**, 2367-72 (2014).

55. Gupta, S., Stamatoyannopoulos, J.A., Bailey, T.L. & Noble, W.S. Quantifying similarity between motifs. *Genome Biol* **8**, R24 (2007).

56. Deplancke, B., Dupuy, D., Vidal, M. & Walhout, A.J. A gateway-compatible yeast one-hybrid system. *Genome Res* **14**, 2093-101 (2004).

57. Pruneda-Paz, J.L. *et al.* A genome-scale resource for the functional characterization of Arabidopsis transcription factors. *Cell Rep* **8**, 622-32 (2014).

58. Gaudinier, A. *et al.* Transcriptional regulation of nitrogen-associated metabolism and growth. *Nature* **563**, 259-264 (2018).

59. Shannon, P. *et al.* Cytoscape: a software environment for integrated models of biomolecular interaction networks. *Genome Res* **13**, 2498-504 (2003).

60. Tian, T. *et al.* agriGO v2.0: a GO analysis toolkit for the agricultural community, 2017 update. *Nucleic Acids Res* (2017).

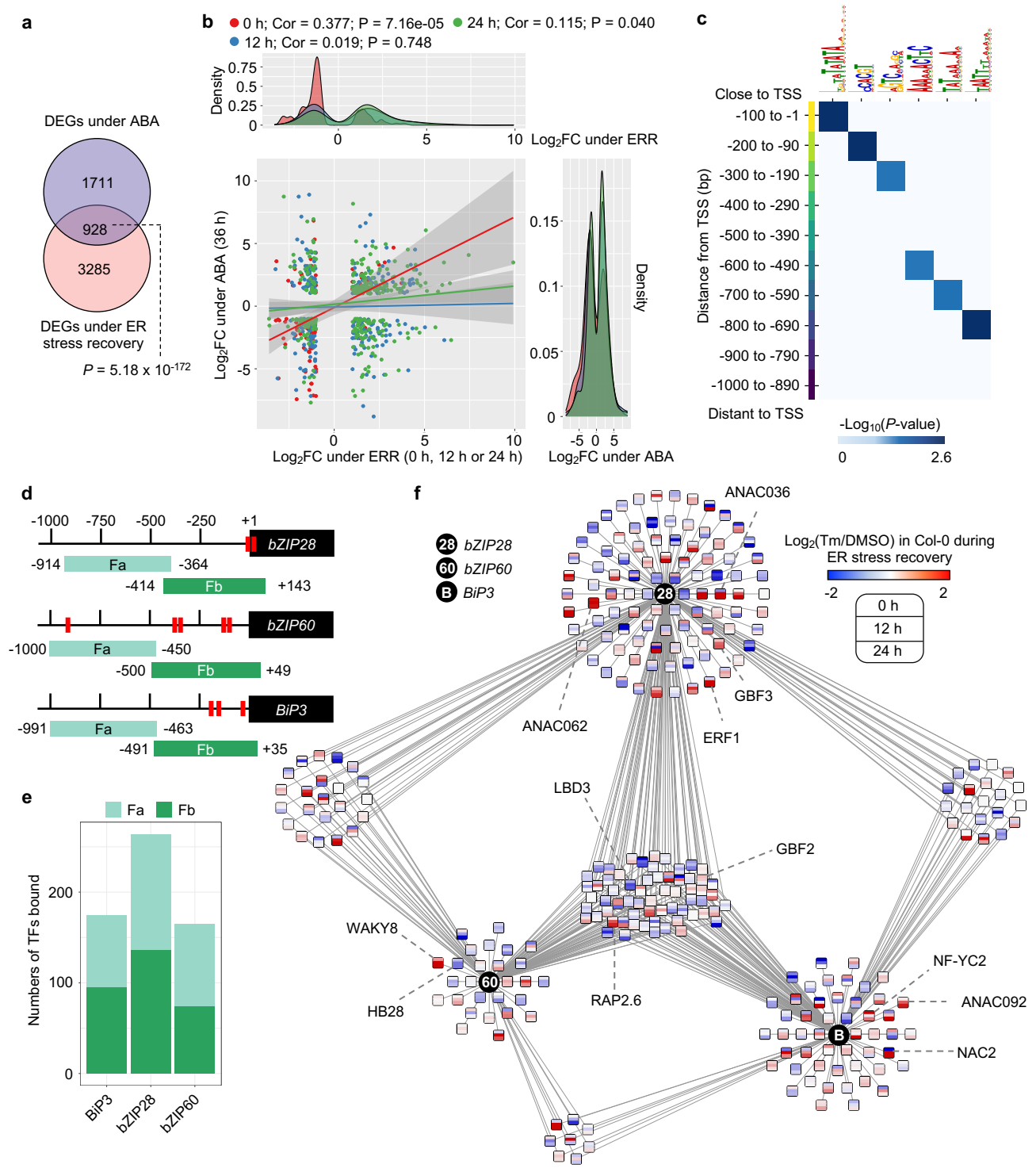
a
DEGs under ABA
1711
928
3285
DEGs under ER stress recovery
P = 5.18 x 10-172
b
0 h; Cor = 0.377; P = 7.16e-05
24 h; Cor = 0.115; P = 0.040
12 h; Cor = 0.019; P = 0.748
Density
Log2FC under ERR
Log2FC under ABA (36 h)
Log2FC under ERR (0 h, 12 h or 24 h)
Log2FC under ABA
c
Close to TSS
Distant to TSS
Distance from TSS (bp)
-100 to -1
-200 to -90
-300 to -190
-400 to -290
-500 to -390
-600 to -490
-700 to -590
-800 to -690
-900 to -790
-1000 to -890
-Log10(P-value)
d
bZIP28
Fa
Fb
bZIP60
BiP3
e
Numbers of TFs bound
BiP3
bZIP28
bZIP60
f
bZIP28
bZIP60
BiP3
Log2(Tm/DMSO) in Col-0 during ER stress recovery
0 h
12 h
24 h
ANAC036
GBF3
ERF1
ANAC062
LBD3
GBF2
WAKY8
HB28
RAP2.6
NF-YC2
ANAC092
NAC2

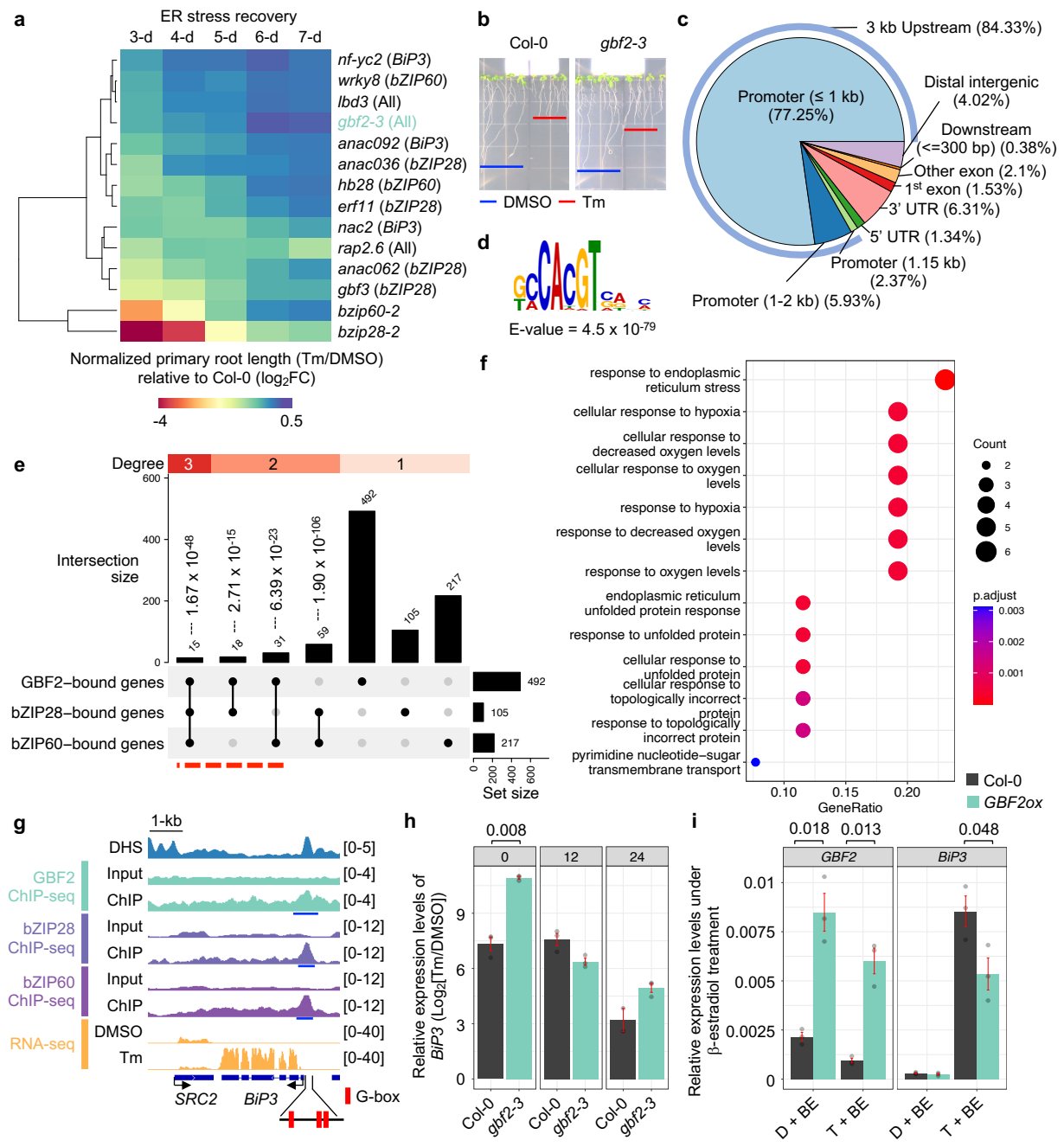
a
ER stress recovery
3-d
4-d
5-d
6-d
7-d
nf-yc2 (BiP3)
wrky8 (bZIP60)
lbd3 (All)
gbf2-3 (All)
anac092 (BiP3)
anac036 (bZIP28)
hb28 (bZIP60)
erf11 (bZIP28)
nac2 (BiP3)
rap2.6 (All)
anac062 (bZIP28)
gbf3 (bZIP28)
bzip60-2
bzip28-2
Normalized primary root length (Tm/DMSO) relative to Col-0 (log2FC)
-4
0.5
b
Col-0
gbf2-3
DMSO
Tm
c
3 kb Upstream (84.33%)
Promoter (≤ 1 kb) (77.25%)
Distal intergenic (4.02%)
Downstream (<=300 bp) (0.38%)
Other exon (2.1%)
1st exon (1.53%)
3' UTR (6.31%)
5' UTR (1.34%)
Promoter (1.15 kb) (2.37%)
Promoter (1-2 kb) (5.93%)
d
E-value = 4.5 x 10-79
e
Degree
3
2
1
Intersection size
1.67 x 10-48
2.71 x 10-15
6.39 x 10-23
1.90 x 10-106
492
105
217
GBF2–bound genes
bZIP28–bound genes
bZIP60–bound genes
Set size
f
response to endoplasmic reticulum stress
cellular response to hypoxia
cellular response to decreased oxygen levels
cellular response to oxygen levels
response to hypoxia
response to decreased oxygen levels
response to oxygen levels
endoplasmic reticulum unfolded protein response
response to unfolded protein
cellular response to unfolded protein
cellular response to topologically incorrect protein
response to topologically incorrect protein
pyrimidine nucleotide−sugar transmembrane transport
GeneRatio
Count
p.adjust
Col-0
GBF2ox
g
1-kb
DHS
GBF2 ChIP-seq
Input
ChIP
bZIP28 ChIP-seq
bZIP60 ChIP-seq
RNA-seq
DMSO
Tm
SRC2
BiP3
G-box
h
Relative expression levels of BiP3 (Log2[Tm/DMSO])
0.008
0
12
24
Col-0
gbf2-3
i
Relative expression levels under β-estradiol treatment
0.018
0.013
0.048
GBF2
BiP3
D + BE
T + BE

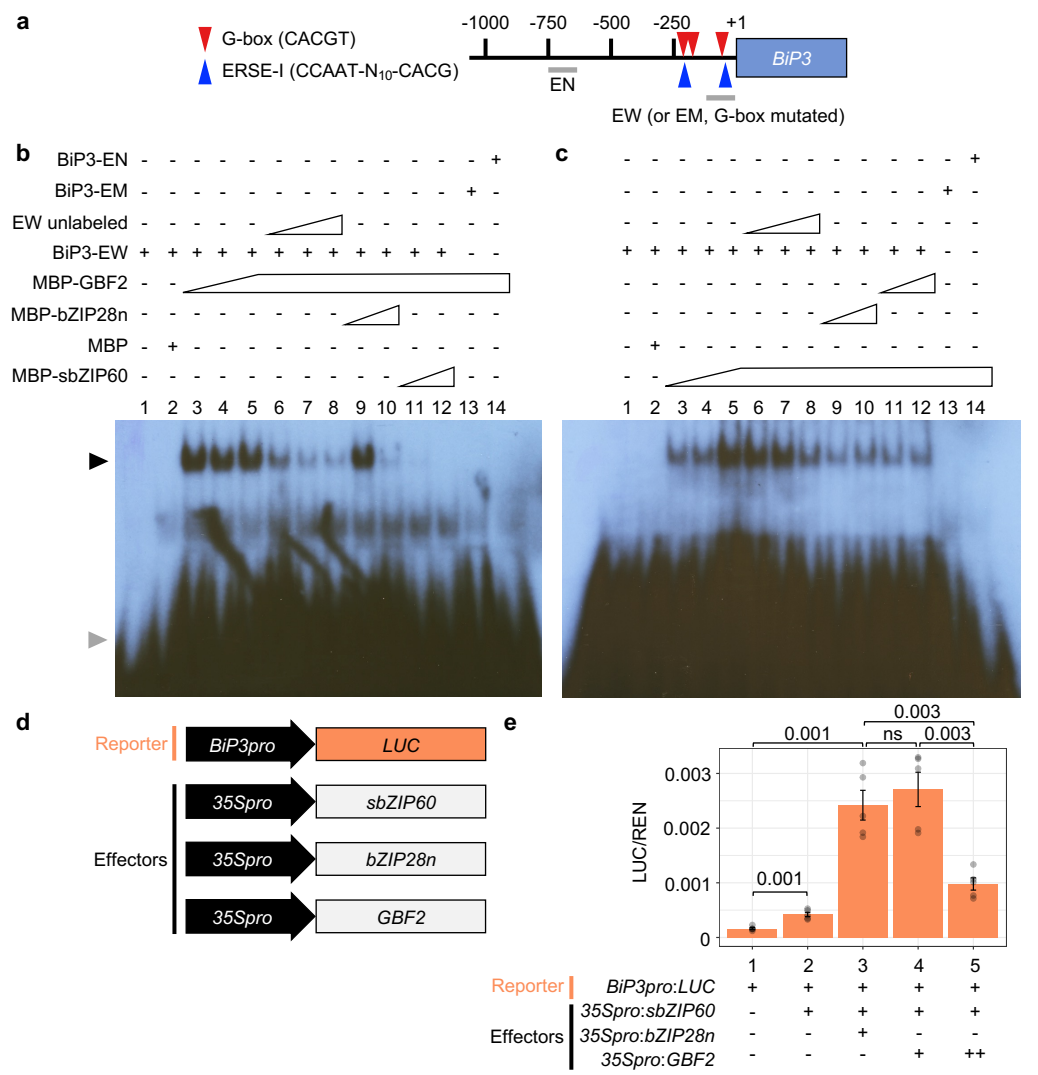
a
G-box (CACGT)
ERSE-I (CCAAT-N10-CACG)
-1000 -750 -500 -250 +1
BiP3
EN
EW (or EM, G-box mutated)
b
BiP3-EN
BiP3-EM
EW unlabeled
BiP3-EW
MBP-GBF2
MBP-bZIP28n
MBP
MBP-sbZIP60
1 2 3 4 5 6 7 8 9 10 11 12 13 14
c
1 2 3 4 5 6 7 8 9 10 11 12 13 14
d
Reporter
BiP3pro
LUC
Effectors
35Spro
sbZIP60
35Spro
bZIP28n
35Spro
GBF2
e
0.001
ns
0.003
0.003
LUC/REN
0.003
0.002
0.001
0
0.001
1 2 3 4 5
Reporter
BiP3pro:LUC + + + + +
Effectors
35Spro:sbZIP60 - + + + +
35Spro:bZIP28n - - + - -
35Spro:GBF2 - - - + ++

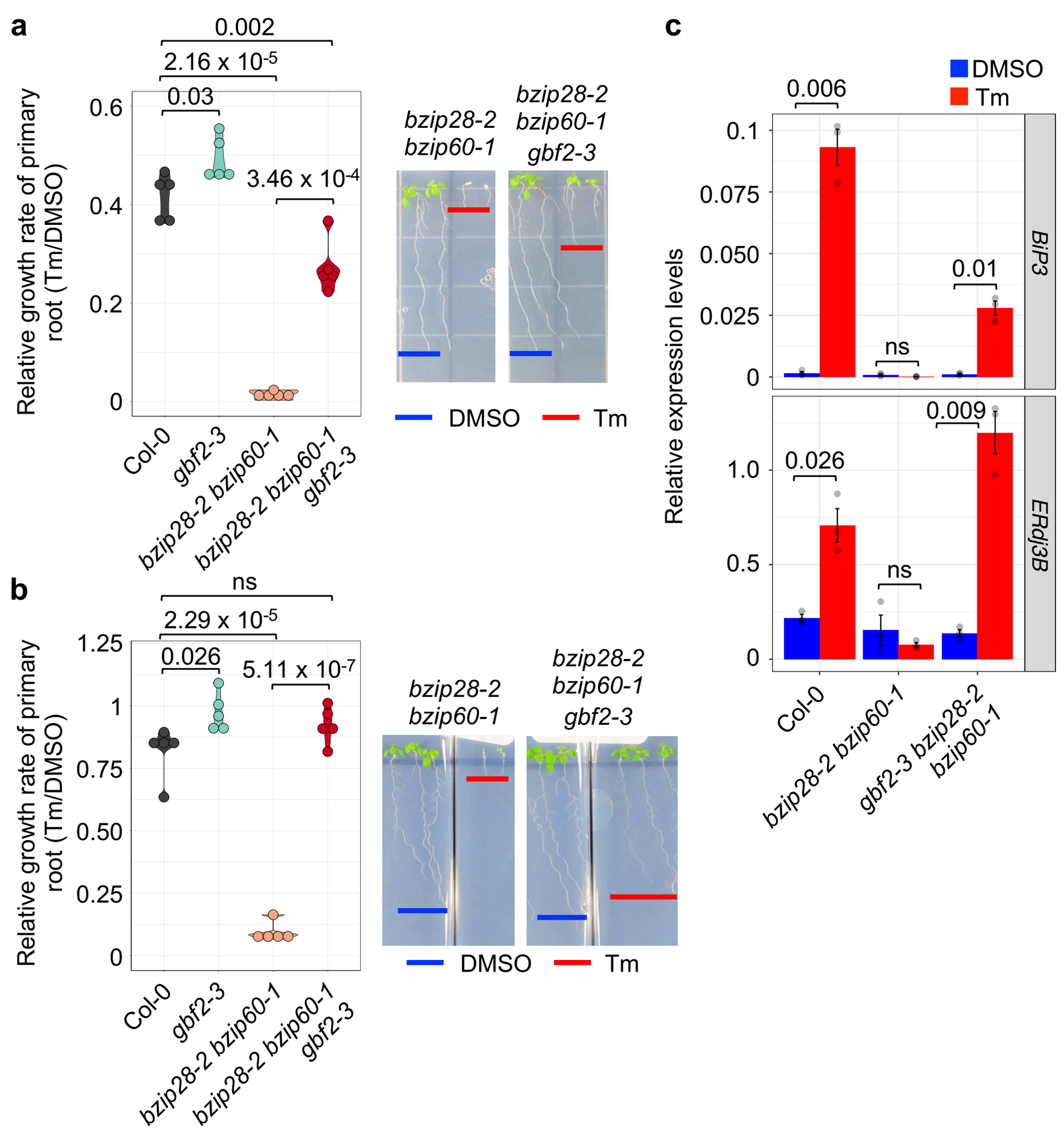
a
0.002
2.16 x 10-5
0.03
3.46 x 10-4
Relative growth rate of primary root (Tm/DMSO)
0.6
0.4
0.2
0
Col-0
gbf2-3
bzip28-2 bzip60-1
bzip28-2 bzip60-1 gbf2-3
bzip28-2 bzip60-1
bzip28-2 bzip60-1 gbf2-3
DMSO
Tm
b
ns
2.29 x 10-5
0.026
5.11 x 10-7
Relative growth rate of primary root (Tm/DMSO)
1.25
1
0.75
0.50
0.25
0
Col-0
gbf2-3
bzip28-2 bzip60-1
bzip28-2 bzip60-1 gbf2-3
bzip28-2 bzip60-1
bzip28-2 bzip60-1 gbf2-3
DMSO
Tm
c
DMSO
Tm
0.006
0.01
ns
BiP3
0.1
0.075
0.050
0.025
0
0.009
0.026
ns
ERdj3B
1.0
0.5
0
Relative expression levels
Col-0
bzip28-2 bzip60-1
gbf2-3 bzip28-2 bzip60-1